Light meson and baryon spectroscopy from charm decays in Fermilab E791

Milind V. Purohit

XXXth International Conference on High Energy Physics

July 26 – August 2, 2000, Osaka.

- $\Lambda_c^+ \to pK^-\pi^+$ 5-dimensional resonant analysis

  Polarization measurement.

- $D_s^+ \to \pi^+\pi^-\pi^+$ Dalitz Plot analysis .

  Study of the width of the $f_0(980)$.

- $D^+ \to \pi^+\pi^-\pi^+$ Dalitz Plot analysis.

  Evidence for the scalar $\sigma(500)$ Meson.

E-781 Spectrometer

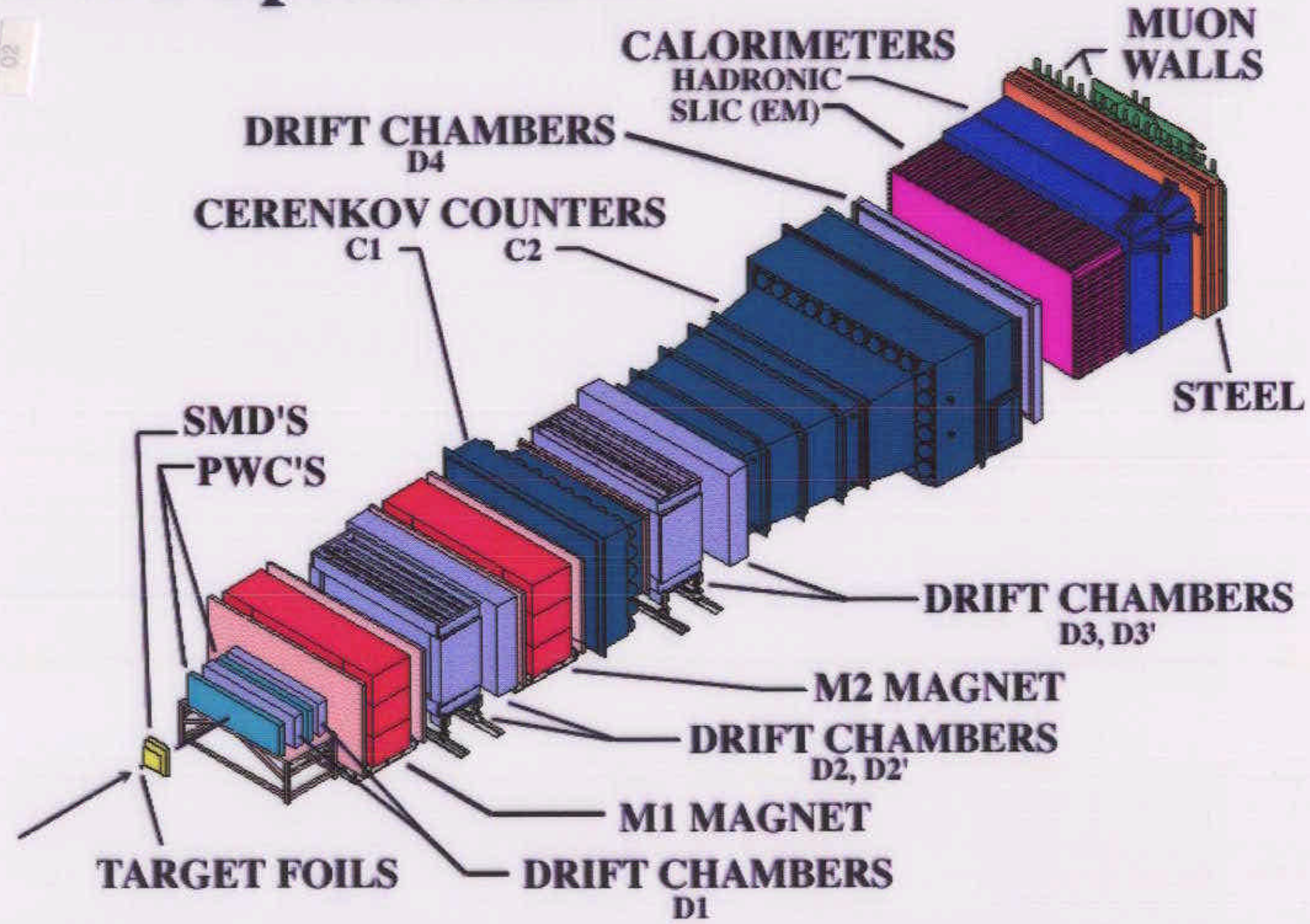

Fermilab E791 Collaboration

CBPF, Rio de Janeiro, Brazil

University of Cincinnati

Fermilab

Kansas State University

University of Mississippi – Oxford

University of South Carolina

Tel Aviv University

University of Wisconsin

University of California – Santa Cruz

CINVESTAV, Mexico

Illinois Institute of Technology

University of Massassachusetts

Universidad Autonoma de Puebla

Stanford University

Tufts University

Yale University

DATA AFTER INITIAL CUTS

E791

Since the KSUSS applied a restriction that SDZ $\geq$ 6.0 and PTBAL $\leq$ 0.4 we also cut any events which violated these boundaries. See figures 6.2 and 6.3 for the real and MC data after the above cuts and reconstructed as pKπ, KKπ, and K$\pi\pi$.

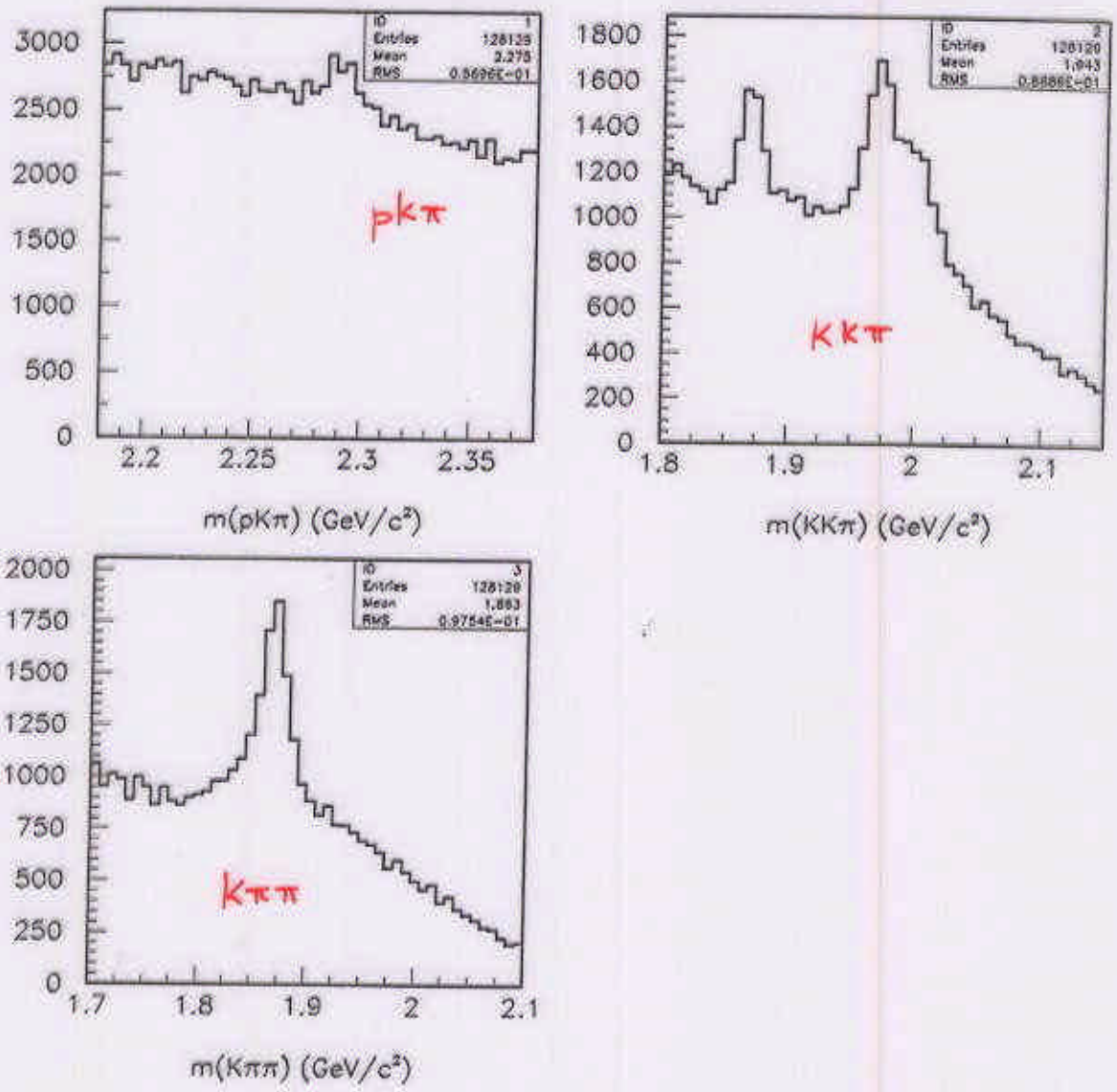

Figure 6.2: Reconstructed masses of real data before Neural Net and D mass cuts.

The last cut we made before using the Neural Net, was to eliminate the D resonances. There are three decays which are more likely to be reconstructed as false $\Lambda_c^+ \to pK^-\pi^+$ than other decays. They are

1. $D^+ \to K^+K^-\pi^+$
2. $D^+ \to K^-\pi^+\pi^+$
3. $D_s^+ \to K^+K^-\pi^+$

Removal of Background: Reflections

E791

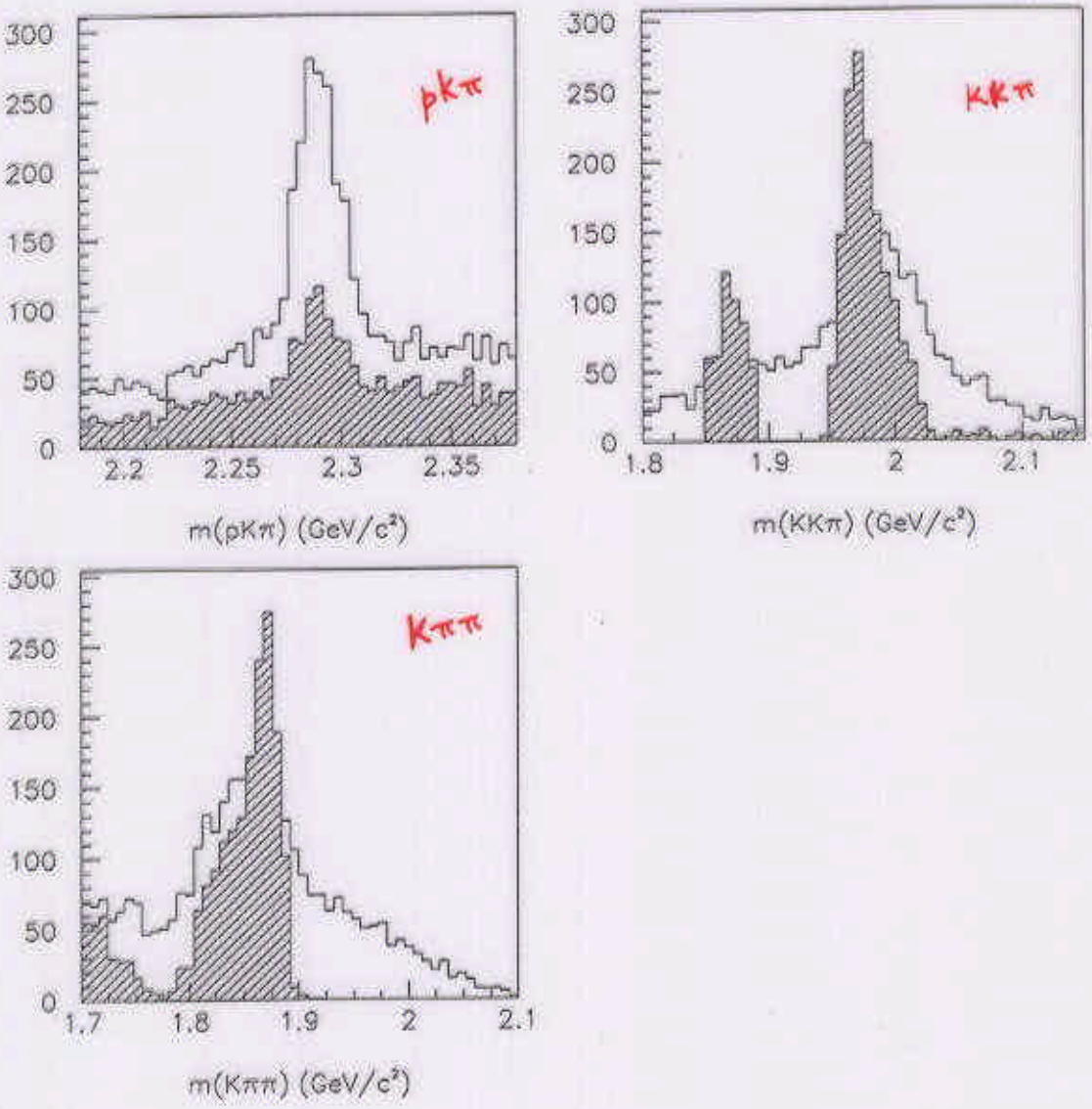

Figure 6.8: Reconstructed masses of real data after the Neural Net cuts are made. The shaded region is the region cut by the D mass cuts. This data set was produced by running the 19,763 events, which were in the D mass range and cut, through the Neural Net cut. The 2137 events of the 19,763 which survived are in the shaded region. These events are not used in the analysis. The larger outline is the total of the D region (2137 events) and the final data set (2271 events).

RESULT OF REFLECTION CUTS

E791

1384.1±48.8 background events and a significance of 20.4σ. See table 6.1 for detail on significance and alternate ways of calculating it.

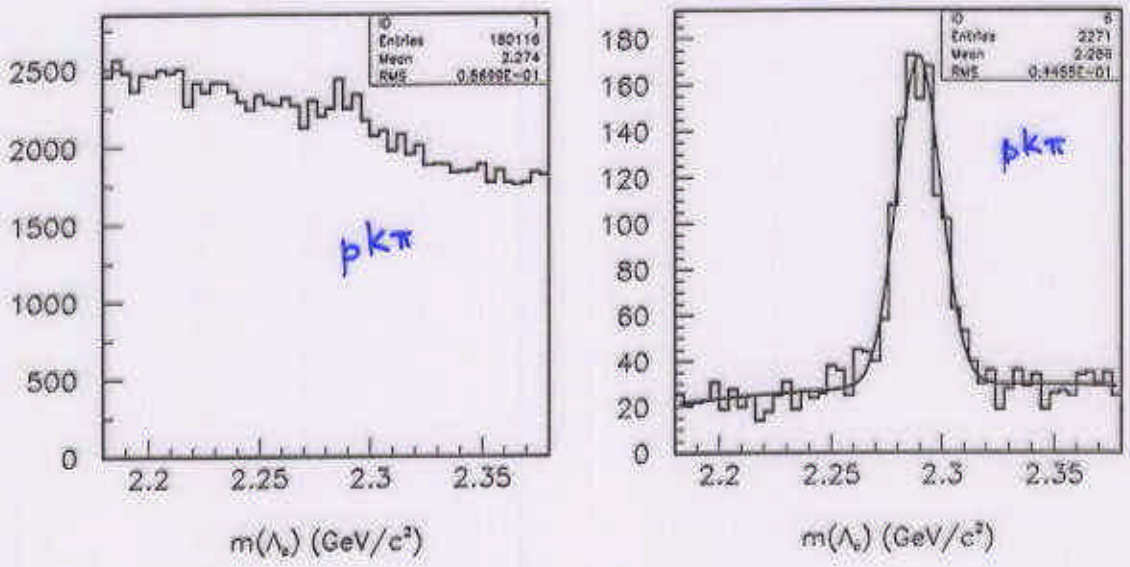

Figure 6.5: (left) Mass(pKπ) of the real data set before Neural Net cuts and (right) after. It has a significance of 20.4σ. There are 886±43 signal events and 1384 background events assuming that the peak is Gaussian, the background is quadratic and the number of signal and background events are variables.

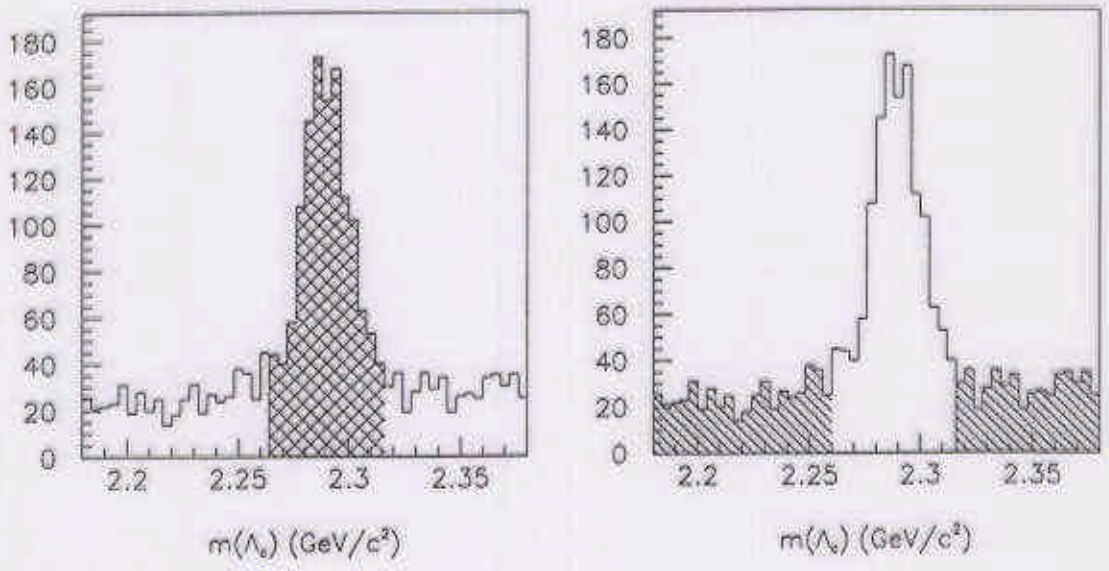

Figure 6.6: Mass(pKπ) of the real data set after the Neural Net cut. For future reference: the shaded area on the left refers to the signal region and on the right to the background regions.

E791 $\Lambda_c^+ \to pK^-\pi^+$ decays

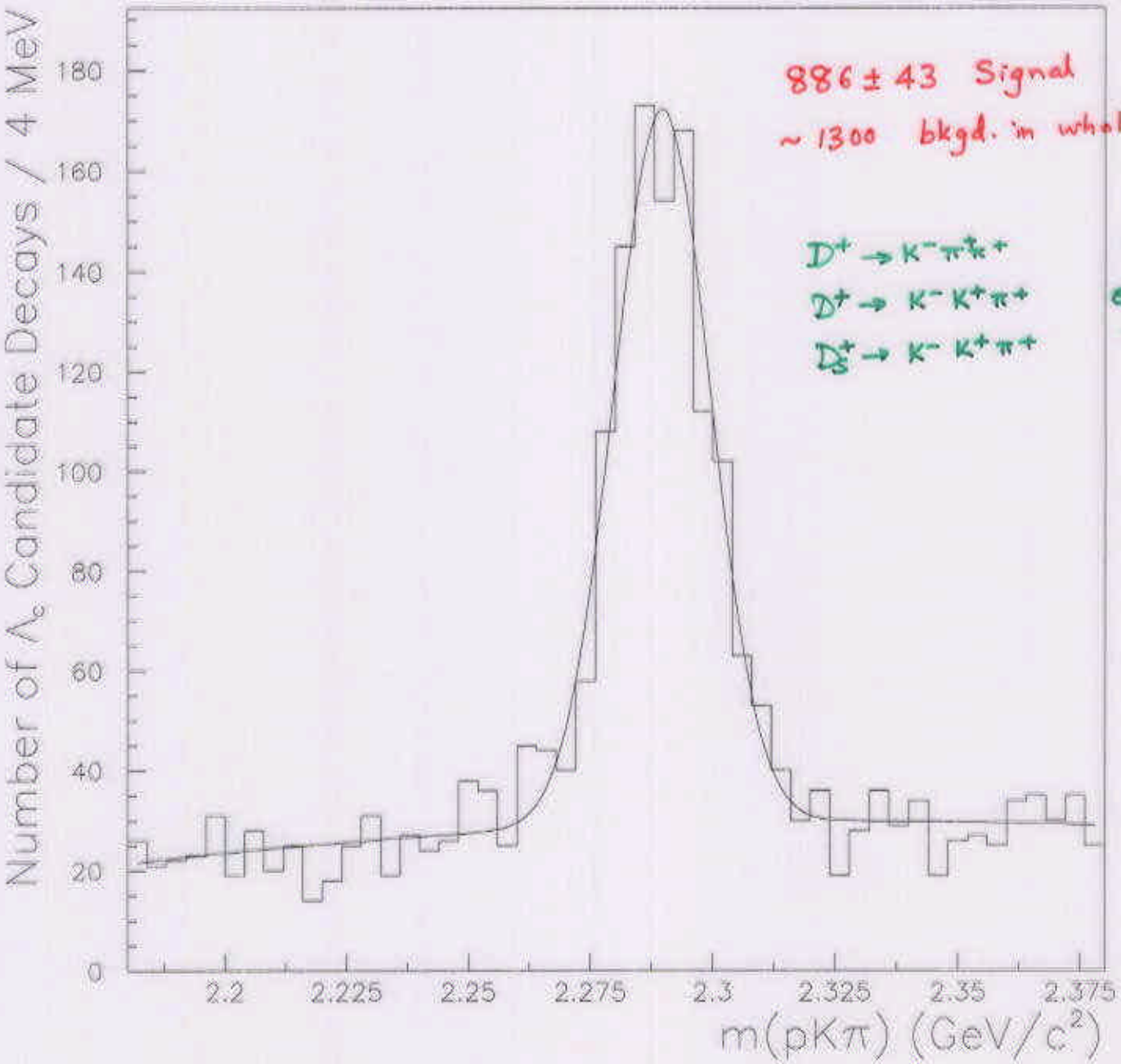

886 ± 43 Signal

~ 1300 bkgd. in whole plot

$D^+ \to K^-\pi^+\pi^+$

$D^+ \to K^-K^+\pi^+$

$D_s^+ \to K^-K^+\pi^+$

Reflections explicitly removed

charm baryon decay rates. The most direct components of the $\Lambda_c^+ \to pK^-\pi^+$ decays (and charge conjugate decays which are implied throughout this paper) include the nonresonant $pK^-\pi^+$ decay, and the $p\overline{K}^{*0}(890)$ and $\Lambda(1520)\pi^+$ two-body decays. All three of these decays can be described by spectator and W-exchange amplitudes. In lowest order, the $\Delta^{++}(1232)K^-$ decay can occur only via the exchange amplitude. Exchange amplitudes are suppressed in charm meson decays, at least at the quark level, because of helicity and form-factor effects. These effects are not expected to inhibit exchange amplitudes for charm baryons due to the three-body nature of the interaction. To understand fully this system of decays, as well as other charmed baryon decays, a complete resonant amplitude analysis is needed.

The charm baryon and its decay products carry spin and the charm baryon may be polarized upon production. Previous charm pseudoscalar meson decay analyses have studied structure in the two-dimensional space of the decay product effective masses (Dalitz plot distributions), but the spin effects just described require five kinematic variables for a complete description. While this complicates the analysis, it affords greater sensitivity to the parameters of interest. As a by-product of the analysis, the production polarization of the Λ_c^+, $\mathbf{P}_{\Lambda_c}$, is also measured. This analysis is the first five dimensional amplitude analysis and, as such, is unique.

2 Formalism

We parameterize the observed decay rate as a function of the Λ_c^+ polarization, $\mathbf{P}_{\Lambda_c}$, and of the amplitudes and relative phases of each intermediate two-body resonance decay. We assume that the nonresonant decay is described by an amplitude that is constant across phase space. The differential decay rate $d\Gamma$ (or signal density S) may be expressed as

$$\begin{aligned} d\Gamma \sim S(\vec{x}) = & \frac{(1+\mathbf{P}_{\Lambda_c})}{2}\left(\left|\sum_r B_r(m_r)\alpha_{r,\frac{1}{2},\frac{1}{2}}\right|^2 + \left|\sum_r B_r(m_r)\alpha_{r,\frac{1}{2},-\frac{1}{2}}\right|^2\right) \\ & + \frac{(1-\mathbf{P}_{\Lambda_c})}{2}\left(\left|\sum_r B_r(m_r)\alpha_{r,-\frac{1}{2},\frac{1}{2}}\right|^2 + \left|\sum_r B_r(m_r)\alpha_{r,-\frac{1}{2},-\frac{1}{2}}\right|^2\right) \quad (1) \end{aligned}$$

where α_{r,m,λ_p} is the complex decay amplitude for resonance r given m, the spin projection of the Λ_c on the z-axis, and λ_p, the proton helicity in the Λ_c rest frame.

$B_r(m_r)$ in Equation 1 is the normalized relativistic Breit-Wigner amplitude

direction of the resonance, r, in the Λ_c rest frame, using the convention of [9]. The primed angles refer to the direction of one of the resonance's daughters in the resonance's rest frame.

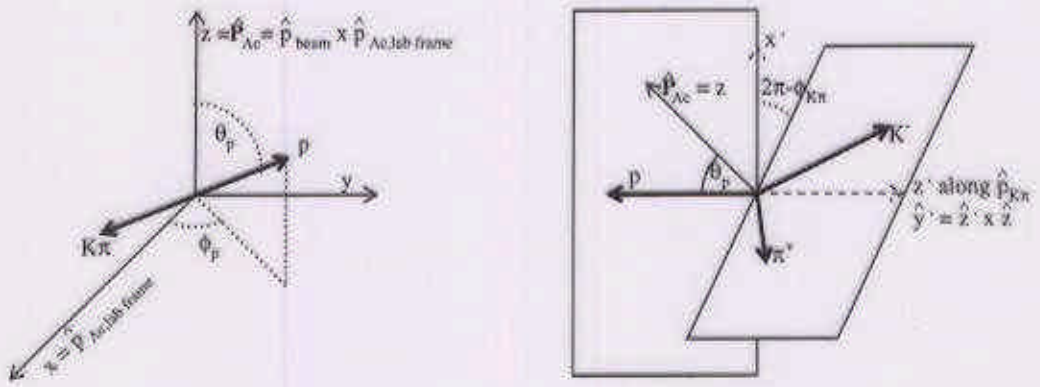

Fig. 1. Definition of angles used in analysis using $\Lambda_c^+ \to p\overline{K^{*0}} \to pK^-\pi^+$ as an example. In both figures the Λ_c^+ is at rest. In the first figure, which defines (θ_p, ϕ_p), the x-axis is along the direction of motion of the Λ_c^+ in the lab frame and the z-axis is the polarization axis, normal to the plane of production. In the second figure we define $\phi_{K\pi}$ which is the angle between the plane containing the $\overline{K^{*0}}$ decay products and the plane containing the proton and the x-axis.

Note that the decay amplitudes for each resonance have contributions to each of the four terms. Each event in the final data sample is described by five kinematic variables of interest (two two-body masses and the decay angles θ_p, ϕ_p, and $\phi_{K\pi}$ as defined in Figure 1) which are determined after the $pK\pi$ reconstructed mass is constrained to the Λ_c mass. We chose the quantization axis (the z-axis in the Λ_c rest frame) to be normal to the Λ_c production plane (as defined by $\hat{p}_{beam} \times \hat{p}_{\Lambda_c}$, where $\hat{p}_{beam}$ is the beam direction and $\hat{p}_{\Lambda_c}$ is the Λ_c production direction in the lab frame). The x-axis in the Λ_c rest frame is chosen to be the direction of the Λ_c in the lab frame.

Table 3
Amplitudes for $\Lambda_c^+(\frac{1}{2}^+) \to (\overline{K}^{*0}(890)(1^-) \to K^-\pi^+)p(\frac{1}{2}^+)$ decay mode.

m	λ_p	Amplitude
$\frac{1}{2}$	$\frac{1}{2}$	$E_1 e^{i\phi_{E_1}} d^{\frac{1}{2}}_{\frac{1}{2}\frac{1}{2}}(\theta_{\overline{K}^{*0}}) d^1_{10}(\theta'_K) e^{i\phi'_K} + E_2 e^{i\phi_{E_2}} d^{\frac{1}{2}}_{\frac{1}{2}-\frac{1}{2}}(\theta_{\overline{K}^{*0}}) d^1_{00}(\theta'_K) e^{i\phi_{\overline{K}^{*0}}}$
$\frac{1}{2}$	$-\frac{1}{2}$	$E_3 e^{i\phi_{E_3}} d^{\frac{1}{2}}_{\frac{1}{2}\frac{1}{2}}(\theta_{\overline{K}^{*0}}) d^1_{00}(\theta'_K) + E_4 e^{i\phi_{E_4}} d^{\frac{1}{2}}_{\frac{1}{2}-\frac{1}{2}}(\theta_{\overline{K}^{*0}}) d^1_{-10}(\theta'_K) e^{i(\phi_{\overline{K}^{*0}} - \phi'_K)}$
$-\frac{1}{2}$	$\frac{1}{2}$	$E_1 e^{i\phi_{E_1}} d^{\frac{1}{2}}_{-\frac{1}{2}\frac{1}{2}}(\theta_{\overline{K}^{*0}}) d^1_{10}(\theta'_K) e^{-i(\phi_{\overline{K}^{*0}} - \phi'_K)} + E_2 e^{i\phi_{E_2}} d^{\frac{1}{2}}_{-\frac{1}{2}-\frac{1}{2}}(\theta_{\overline{K}^{*0}}) d^1_{00}(\theta'_K)$
$-\frac{1}{2}$	$-\frac{1}{2}$	$E_3 e^{i\phi_{E_3}} d^{\frac{1}{2}}_{-\frac{1}{2}\frac{1}{2}}(\theta_{\overline{K}^{*0}}) d^1_{00}(\theta'_K) e^{-i\phi_{\overline{K}^{*0}}} + E_4 e^{i\phi_{E_4}} d^{\frac{1}{2}}_{-\frac{1}{2}-\frac{1}{2}}(\theta_{\overline{K}^{*0}}) d^1_{-10}(\theta'_K) e^{-i\phi'_K}$

corrected for the centrifugal barrier[3]. Given the decay mode $\Lambda_c \to r(\to ab)c$,

$$B_r(m_r) = (-2|p_c||p_a|)^L \frac{F_{\Lambda_c} F_r}{m_0^2 - m_r^2 - i m_0 \Gamma_r} \tag{2}$$

where

$$\Gamma_r = \Gamma_0 (\frac{q}{q_0})^{2L+1} \frac{m_0}{m_r} \frac{F_r^2(q)}{F_r^2(q_0)} \tag{3}$$

for resonance r at the reconstructed two body mass m_r, with the momentum q (and q_0 when $m_r = m_0$) of a daughter particle in the resonance's rest frame, and with resonance mass and width m_0 and Γ_0 as found in [2]. Using this convention, we set $B_r(m_r)$ for the nonresonant decay to be 1.0. F_L is the strong coupling factor at the appropriate decay vertex, and is in the Blatt-Weisskopf form as described in table 1 below. Table 2 lists the range of the strong interaction, R_X.

Table 1
We list here the expressions for F and values of R used in the Breit-Wigner amplitude.

L	F_L
0	1
1	$(1 + R_X^2 q^2)^{-1/2}$
2	$(9 + 3R_X^2 q^2 + R_X^4 q^4)^{-1/2}$

Table 2
We list here the expressions for F and values of R used in the Breit-Wigner amplitude.

X	R_X $(\mathrm{GeV}/c^2)^{-1}$
$\overline{K}^{*0}(890)$	3.4 [4]
$\Delta^{++}(1232)$	5.22 [5]
$\Lambda(1520)$	6.29 [6]
Λ_c^+	5.07 [7]

In Tables 3–6, where the amplitudes α_{r,m,λ_p} (derived using the helicity formalism described in [8]) can be seen more explicitly, the direction (ϕ_r, θ_r) is the

Table 4
Amplitudes for $\Lambda_c^+(\frac{1}{2}^+) \to (\Delta^{++}(1232)(\frac{3}{2}^+) \to p\pi^+)K^-$ decay mode.

m	λ_p	Amplitude
$\frac{1}{2}$	$\frac{1}{2}$	$F_1 e^{i\phi_{F_1}} d^{\frac{1}{2}}_{\frac{1}{2}\frac{1}{2}}(\theta_{\Delta^{++}}) d^{\frac{3}{2}}_{\frac{1}{2}\frac{1}{2}}(\theta'_p) + F_2 e^{i\phi_{F_2}} d^{\frac{1}{2}}_{\frac{1}{2}-\frac{1}{2}}(\theta_{\Delta^{++}}) d^{\frac{3}{2}}_{-\frac{1}{2}\frac{1}{2}}(\theta'_p) e^{i(\phi_{\Delta^{++}}-\phi'_p)}$
$\frac{1}{2}$	$-\frac{1}{2}$	$F_1 e^{i\phi_{F_1}} d^{\frac{1}{2}}_{\frac{1}{2}\frac{1}{2}}(\theta_{\Delta^{++}}) d^{\frac{3}{2}}_{\frac{1}{2}-\frac{1}{2}}(\theta'_p) e^{i\phi'_p} + F_2 e^{i\phi_{F_2}} d^{\frac{1}{2}}_{\frac{1}{2}-\frac{1}{2}}(\theta_{\Delta^{++}}) d^{\frac{3}{2}}_{-\frac{1}{2}-\frac{1}{2}}(\theta'_p) e^{i\phi_{\Delta^{++}}}$
$-\frac{1}{2}$	$\frac{1}{2}$	$F_1 e^{i\phi_{F_1}} d^{\frac{1}{2}}_{-\frac{1}{2}\frac{1}{2}}(\theta_{\Delta^{++}}) d^{\frac{3}{2}}_{\frac{1}{2}\frac{1}{2}}(\theta'_p) e^{-i\phi_{\Delta^{++}}} + F_2 e^{i\phi_{F_2}} d^{\frac{1}{2}}_{-\frac{1}{2}-\frac{1}{2}}(\theta_{\Delta^{++}}) d^{\frac{3}{2}}_{-\frac{1}{2}\frac{1}{2}}(\theta'_p) e^{-i\phi'_p}$
$-\frac{1}{2}$	$-\frac{1}{2}$	$F_1 e^{i\phi_{F_1}} d^{\frac{1}{2}}_{-\frac{1}{2}\frac{1}{2}}(\theta_{\Delta^{++}}) d^{\frac{3}{2}}_{\frac{1}{2}-\frac{1}{2}}(\theta'_p) e^{-i(\phi_{\Delta^{++}}-\phi'_p)} + F_2 e^{i\phi_{F_2}} d^{\frac{1}{2}}_{-\frac{1}{2}-\frac{1}{2}}(\theta_{\Delta^{++}}) d^{\frac{3}{2}}_{-\frac{1}{2}-\frac{1}{2}}(\theta'_p)$

Table 5
Amplitudes for $\Lambda_c^+(\frac{1}{2}^+) \to (\Lambda(1520)(\frac{3}{2}^-) \to pK^-)\pi^+$ decay mode.

m	λ_p	Amplitude
$\frac{1}{2}$	$\frac{1}{2}$	$H_1 e^{i\phi_{H_1}} d^{\frac{1}{2}}_{\frac{1}{2}\frac{1}{2}}(\theta_{\Lambda(1520)}) d^{\frac{3}{2}}_{\frac{1}{2}\frac{1}{2}}(\theta'_p) + H_2 e^{i\phi_{H_2}} d^{\frac{1}{2}}_{\frac{1}{2}-\frac{1}{2}}(\theta_{\Lambda(1520)}) d^{\frac{3}{2}}_{-\frac{1}{2}\frac{1}{2}}(\theta'_p) e^{i(\phi_{\Lambda(1520)}-\phi'_p)}$
$\frac{1}{2}$	$-\frac{1}{2}$	$-(H_1 e^{i\phi_{H_1}} d^{\frac{1}{2}}_{\frac{1}{2}\frac{1}{2}}(\theta_{\Lambda(1520)}) d^{\frac{3}{2}}_{\frac{1}{2}-\frac{1}{2}}(\theta'_p) e^{i\phi'_p} + H_2 e^{i\phi_{H_2}} d^{\frac{1}{2}}_{\frac{1}{2}-\frac{1}{2}}(\theta_{\Lambda(1520)}) d^{\frac{3}{2}}_{-\frac{1}{2}-\frac{1}{2}}(\theta'_p) e^{i\phi_{\Lambda(1520)}})$
$-\frac{1}{2}$	$\frac{1}{2}$	$H_1 e^{i\phi_{H_1}} d^{\frac{1}{2}}_{-\frac{1}{2}\frac{1}{2}}(\theta_{\Lambda(1520)}) d^{\frac{3}{2}}_{\frac{1}{2}\frac{1}{2}}(\theta'_p) e^{-i\phi_{\Lambda(1520)}} + H_2 e^{i\phi_{H_2}} d^{\frac{1}{2}}_{-\frac{1}{2}-\frac{1}{2}}(\theta_{\Lambda(1520)}) d^{\frac{3}{2}}_{-\frac{1}{2}\frac{1}{2}}(\theta'_p) e^{-i\phi'_p}$
$-\frac{1}{2}$	$-\frac{1}{2}$	$-(H_1 e^{i\phi_{H_1}} d^{\frac{1}{2}}_{-\frac{1}{2}\frac{1}{2}}(\theta_{\Lambda(1520)}) d^{\frac{3}{2}}_{\frac{1}{2}-\frac{1}{2}}(\theta'_p) e^{-i(\phi_{\Lambda(1520)}-\phi'_p)} + H_2 e^{i\phi_{H_2}} d^{\frac{1}{2}}_{-\frac{1}{2}-\frac{1}{2}}(\theta_{\Lambda(1520)}) d^{\frac{3}{2}}_{-\frac{1}{2}-\frac{1}{2}}(\theta'_p))$

Table 6
Amplitudes for nonresonant $\Lambda_c^+(\frac{1}{2}^+) \to pK^-\pi^+$ decay mode.

m	λ_p	Amplitude
$\frac{1}{2}$	$\frac{1}{2}$	$N_{++} e^{i\phi_{N_{++}}}$
$\frac{1}{2}$	$-\frac{1}{2}$	$N_{+-} e^{i\phi_{N_{+-}}}$
$-\frac{1}{2}$	$\frac{1}{2}$	$N_{-+} e^{i\phi_{N_{-+}}}$
$-\frac{1}{2}$	$-\frac{1}{2}$	$N_{--} e^{i\phi_{N_{--}}}$

3 Experiment E791 and Data Reduction

We analyze data from Fermilab fixed-target experiment E791, which ran from 1991–1992. The data were recorded from 500 GeV/c π^- beam interactions in five thin target foils (one platinum, four diamond) whose centers were separated by about 1.53 cm. The detector, described elsewhere in more detail[10,11], was a large-acceptance, forward, two-magnet spectrometer. Its key components for this study included eight planes of multiwire proportional chambers, and six planes of silicon microstrip detectors (SMD) before the target for beam tracking, a 17-plane SMD system and 35 drift chamber planes downstream of the target for track and vertex reconstruction, and two multicell threshold Čerenkov counters for charged particle identification.

An unrestrictive, open-charm event selection based on total transverse energy

$\Lambda_c^+ \to p K^- \pi^+$

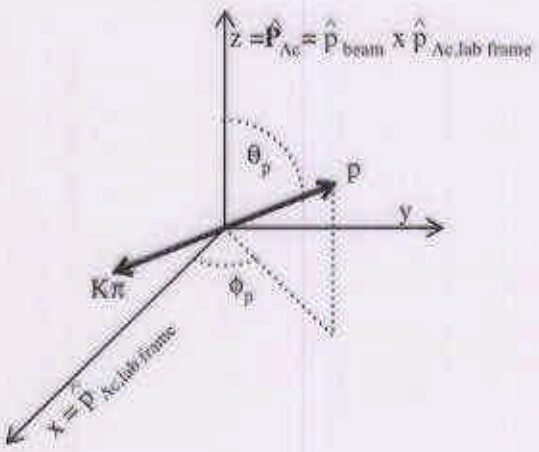

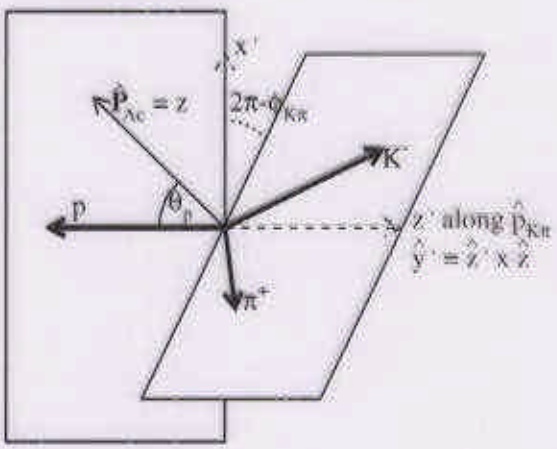

Spectator

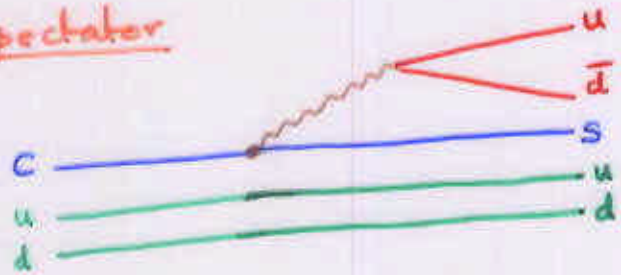

e.g., $p\bar{K}^{*0}$

Exchange

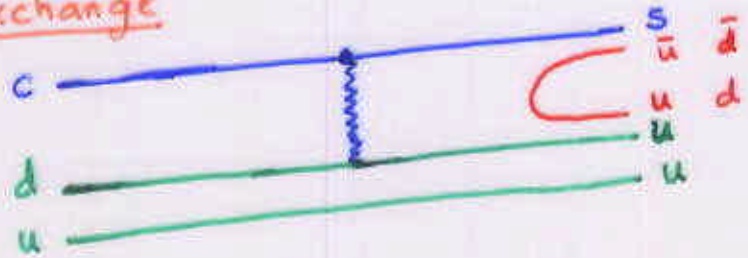

e.g., $p\overline{K^{*0}}$, $\Delta^{++} K^-$

ACCEPTANCE MODEL E791

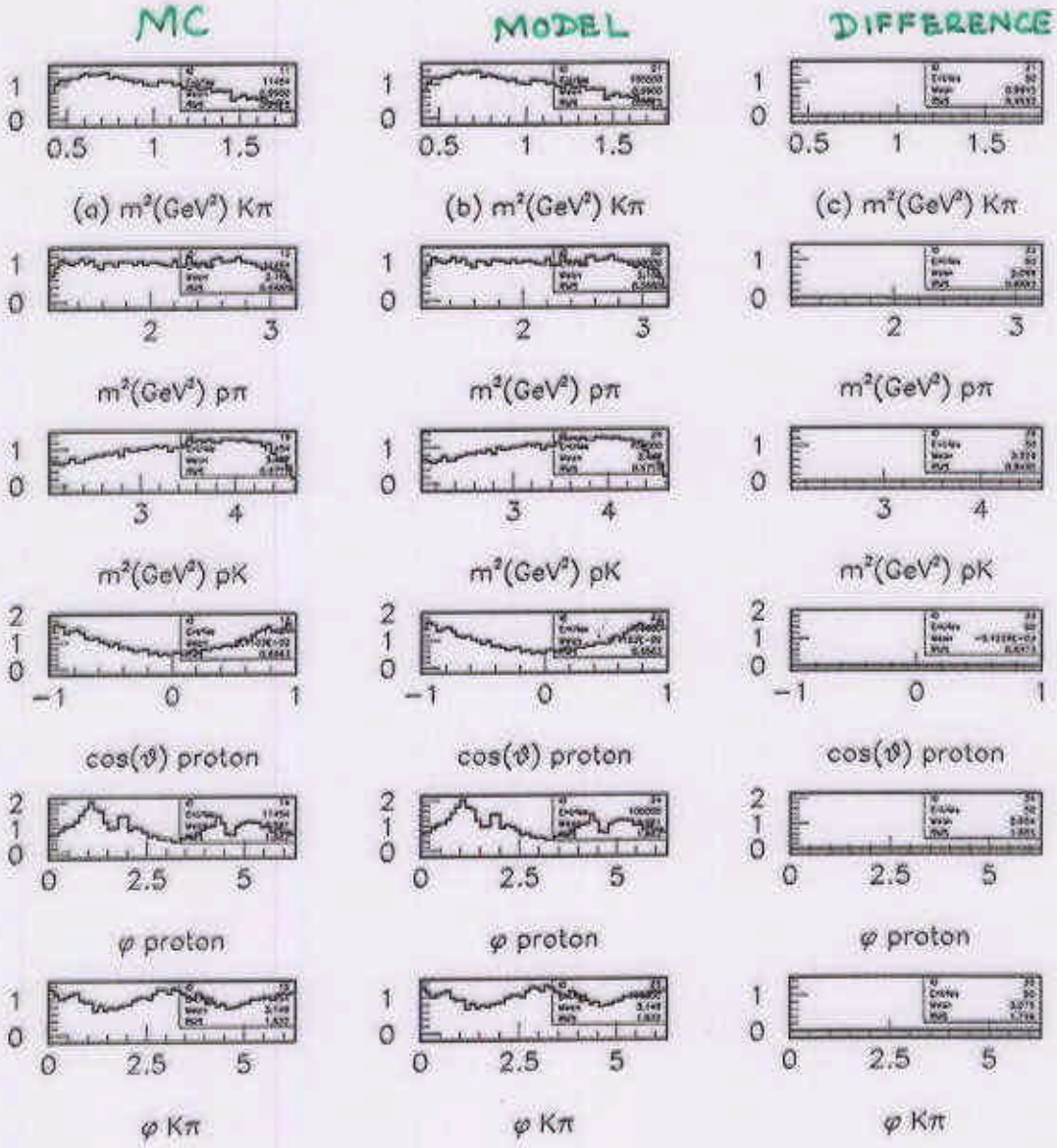

Figure 8.7: Acceptance. (a) The one dimensional projections of the surviving Monte Carlo divided by uniform phase space, (b) The model of the acceptance, (c) the difference between the real acceptance and the model.

BACKGROUND MODEL

E791

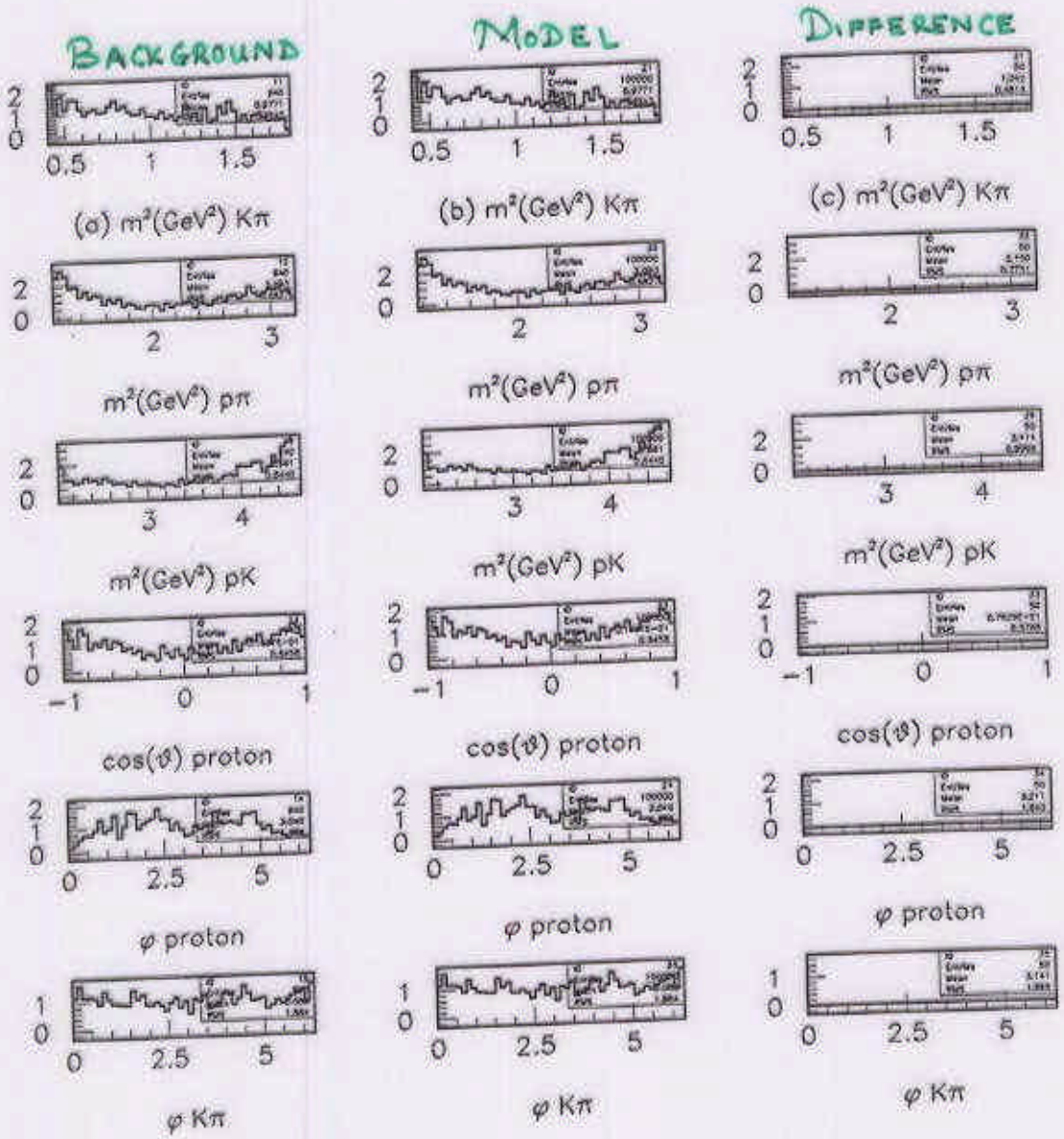

Figure 8.8: Background. (a) The one dimensional projections of the background divided by uniform phase space, (b) The model of the background, (c) the difference between the real background and the model.

E791 VERY PRELIMINARY

$\Lambda_c^+ \to pK^-\pi^+$

Table 5
Decay amplitudes and polarization and mass plot parameters for $\Lambda_c \to pK\pi$ from the MINUIT fit with statistical errors.

FIT RESULTS

Terms	Parameter	Value
$pK^{*0}(890)$	E_1	0.52± 0.17
	ϕ_{E_1}	-1.01± 0.48
	E_2	0.20± 0.10
	ϕ_{E_2}	2.35± 0.67
	E_3	0.21± 0.10
	ϕ_{E_3}	3.46± 0.42
	E_4	0.16± 0.10
	ϕ_{E_4}	5.29± 0.55
$\Delta^{++}(1232)K^-$	F_1	0.17± 0.07
	ϕ_{F_1}	4.98± 0.41
	F_2	0.38± 0.13
	ϕ_{F_2}	4.88± 0.40
$\Lambda^*(1520)\pi^+$	H_1	0.18± 0.09
	ϕ_{H_1}	5.93± 0.52
	H_2	0.20± 0.07
	ϕ_{H_2}	-0.06± 0.55
Nonresonant	N_{++}	0.46± 0.26
	$\phi_{N_{++}}$	3.48± 0.54
	N_{+-}	1.00
	$\phi_{N_{+-}}$	0.00
	N_{-+}	0.18± 0.15
	$\phi_{N_{-+}}$	0.75± 0.71
	N_{--}	0.94± 0.45
	$\phi_{N_{--}}$	1.13± 0.36
Polarization (bin 1)	$\mathbf{P}_{\Lambda_c,1}$	0.15± 0.21
Polarization (bin 2)	$\mathbf{P}_{\Lambda_c,2}$	-0.22± 0.25
Polarization (bin 3)	$\mathbf{P}_{\Lambda_c,3}$	-0.67± 0.15
# Signal Events	n_s	946± 38
# Background Events	n_b	1324± 43
Background Quad Term	b_q	-0.98± 10.51
Background Linear Term	b_l	1.34± 0.48
Mass_{Λ_c} (GeV/c^2)	m_0	2.29± 0.00
Width_{Λ_c} (MeV/c^2)	σ_l	20.1± 4.8
Width_{Λ_c} (MeV/c^2)	σ_c	9.3± 0.6

E791 VERY PRELIMINARY

16

$\Lambda_c^+ \to pK^-\pi^+$

Table 6
The systematic errors on fit fractions.

Mode	Drift Chamber (%)	Čerenkov Counter (%)	Acceptance Adjust (%)	Production Model (%)	Combined Error (%)
$p\bar{K}^{*0}(890)$	1.7	0.6	0.3	0.0	1.8
$\Delta^{++}(1232)K^-$	2.5	1.2	0.7	0.1	2.9
$\Lambda(1520)\pi^+$	0.9	0.5	0.4	0.1	1.1
Nonresonant	3.2	1.1	0.9	0.1	3.5

Table 7
The decay fractions for $\Lambda_c^+ \to pK^-\pi^+$ with statistical and systematic errors from the final fit.

Mode	Fit Fraction (%)
$p\bar{K}^{*0}(890)$	19.5±2.6±1.8
$\Delta^{++}(1232)K^-$	18.0±2.9±2.9
$\Lambda(1520)\pi^+$	7.7±1.8±1.1
Nonresonant	54.8±5.5±3.5

FIT FRACTIONS

uncertainties are comparable because of our more general fit.

Table 8
Λ_c branching ratios relative to the inclusive $\Lambda_c^+ \to pK^-\pi^+$ branching fraction. The NA32 and ISR values were calculated from one-dimensional projections only.

Mode	E791	NA32[14]	ISR[15]
$p\bar{K}^{*0}(890)$	0.29±0.04±0.03	$0.35^{+0.06}_{-0.07}$±0.03	0.42±0.24
$\Delta^{++}(1232)K^-$	0.18±0.03±0.03	$0.12^{+0.04}_{-0.05}$±0.05	0.40±0.17
$\Lambda(1520)\pi$	0.15±0.04±0.02	$0.09^{+0.04}_{-0.03}$±0.02	
Nonresonant	0.55±0.06±0.04	$0.56^{+0.07}_{-0.09}$±0.05	

B.R.

5 Discussion and Conclusions

Significant resonant and non-resonant branching fractions are found in this analysis of a 20σ $\Lambda_c^+ \to pK^-\pi^+$ signal, the largest sample so far analyzed. The size of the sample allows for inclusion of relative phases of the various contributions and a full accounting of spin and production polarization for the first time in such an analysis. The $\Delta(1232)^{++}K^-$ and $\Lambda(1520)\pi^+$ decay modes are seen as statistically significant contributions for the first time, even when uncertainties associated with phases and other variables are included. The

E791 $\Lambda_c^+ \to pK^-\pi^+$ DECAY PROJECTIONS

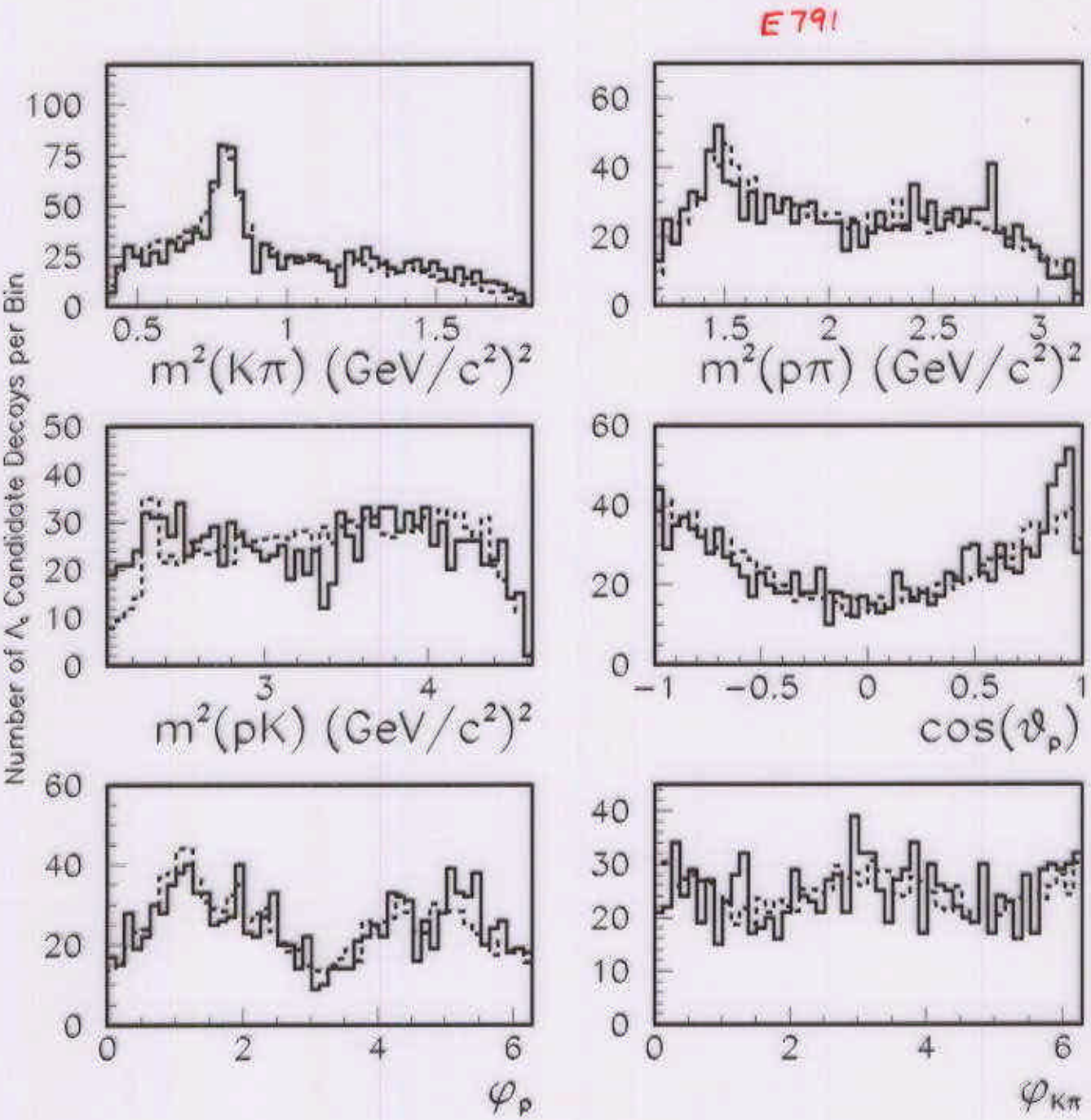

E791 PRELIMINARY

$\Lambda_c^+ \to pK^-\pi^+$

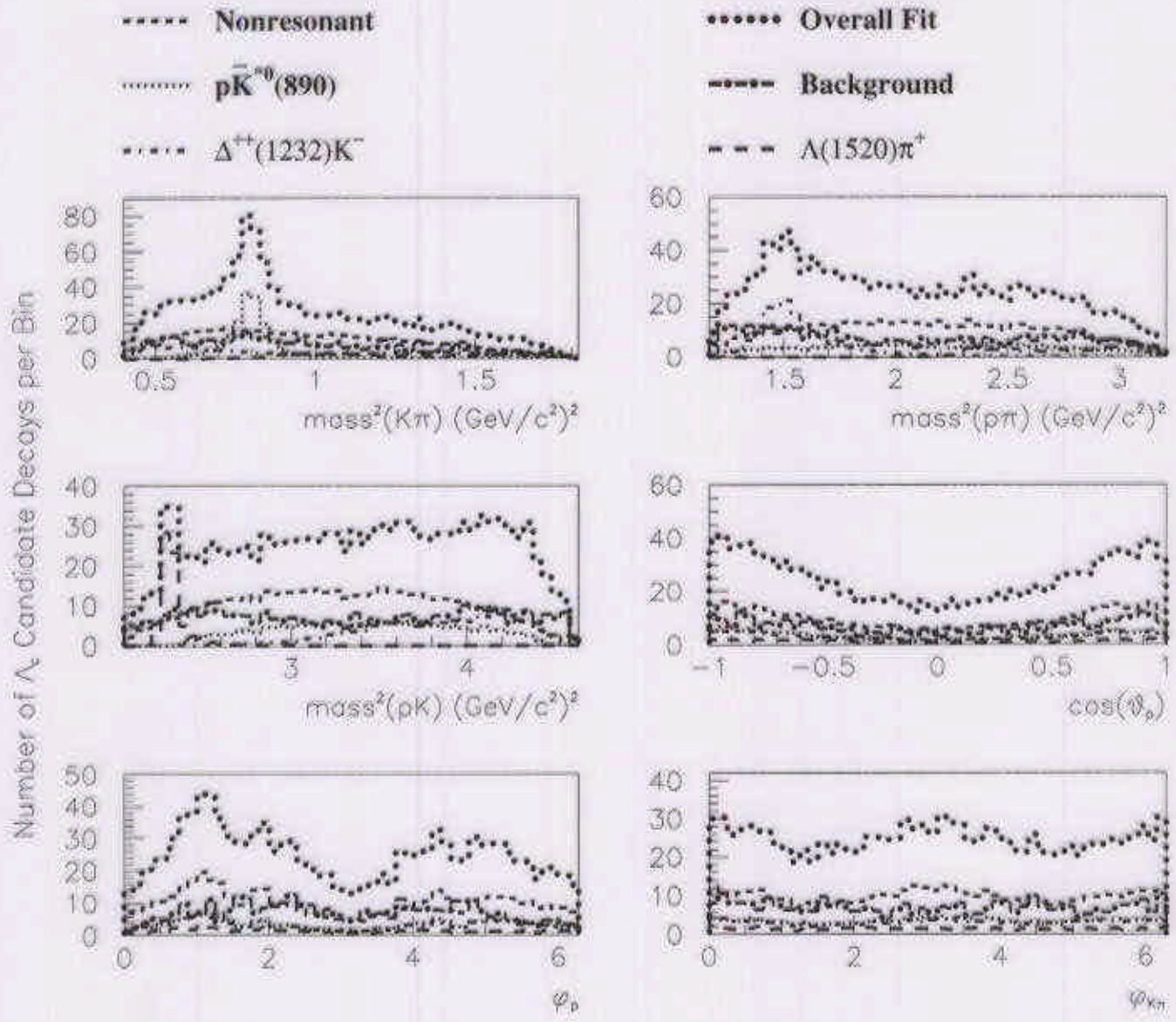

E791

$\Lambda_c^+ \to \Sigma^{*-}(\to pK^-)\pi^+$ INCLUSION

$m = 1556 \pm 19$ MeV/c^2
$\Gamma = 279 \pm 74$ MeV/c^2

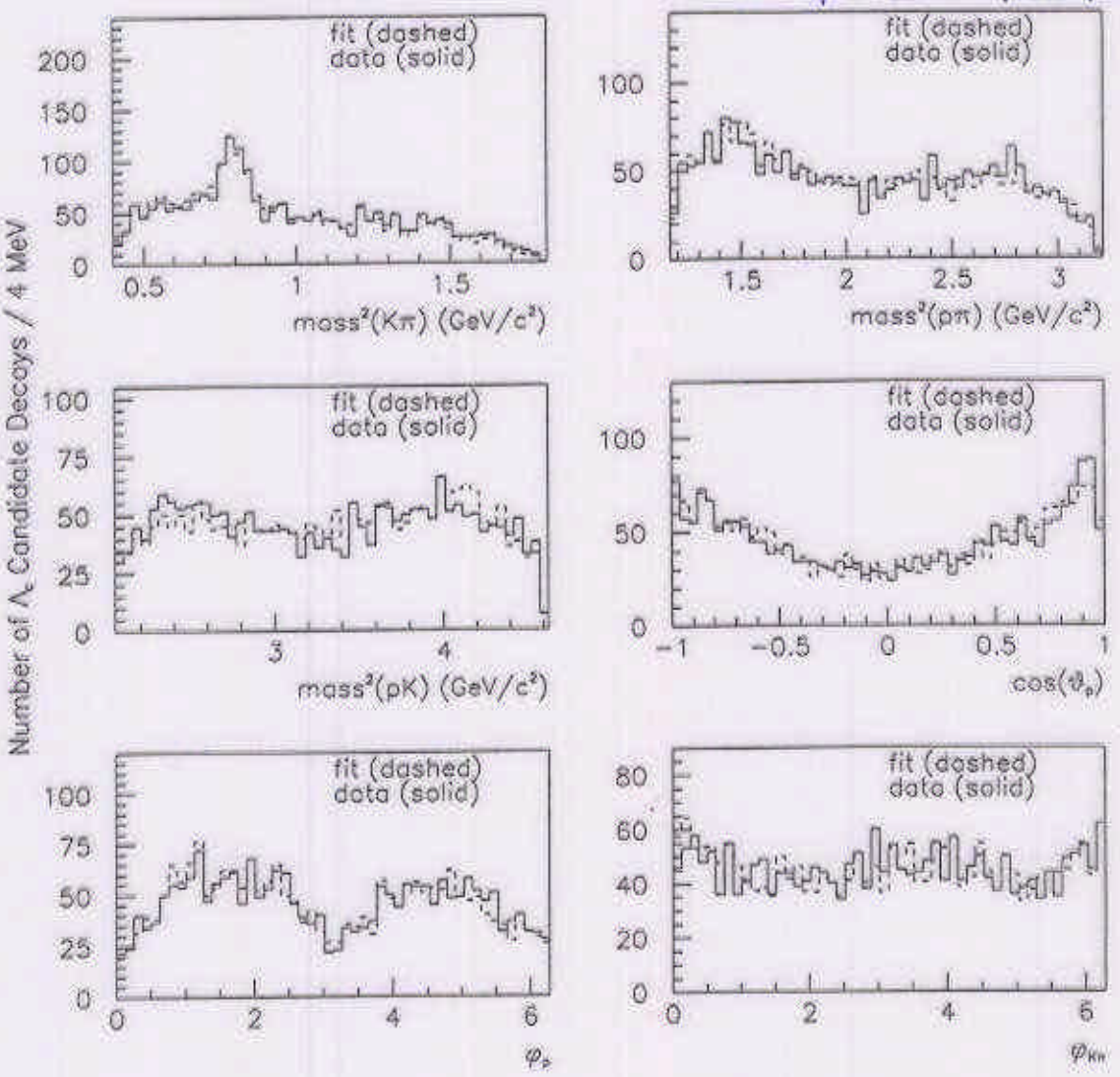

Figure K.1: The one dimensional projections of the new fit and real data.

ALSO POSSIBLE: TAIL OF $\Lambda(1405) \to pK^-$

Λ_c Polarization vs. p_T

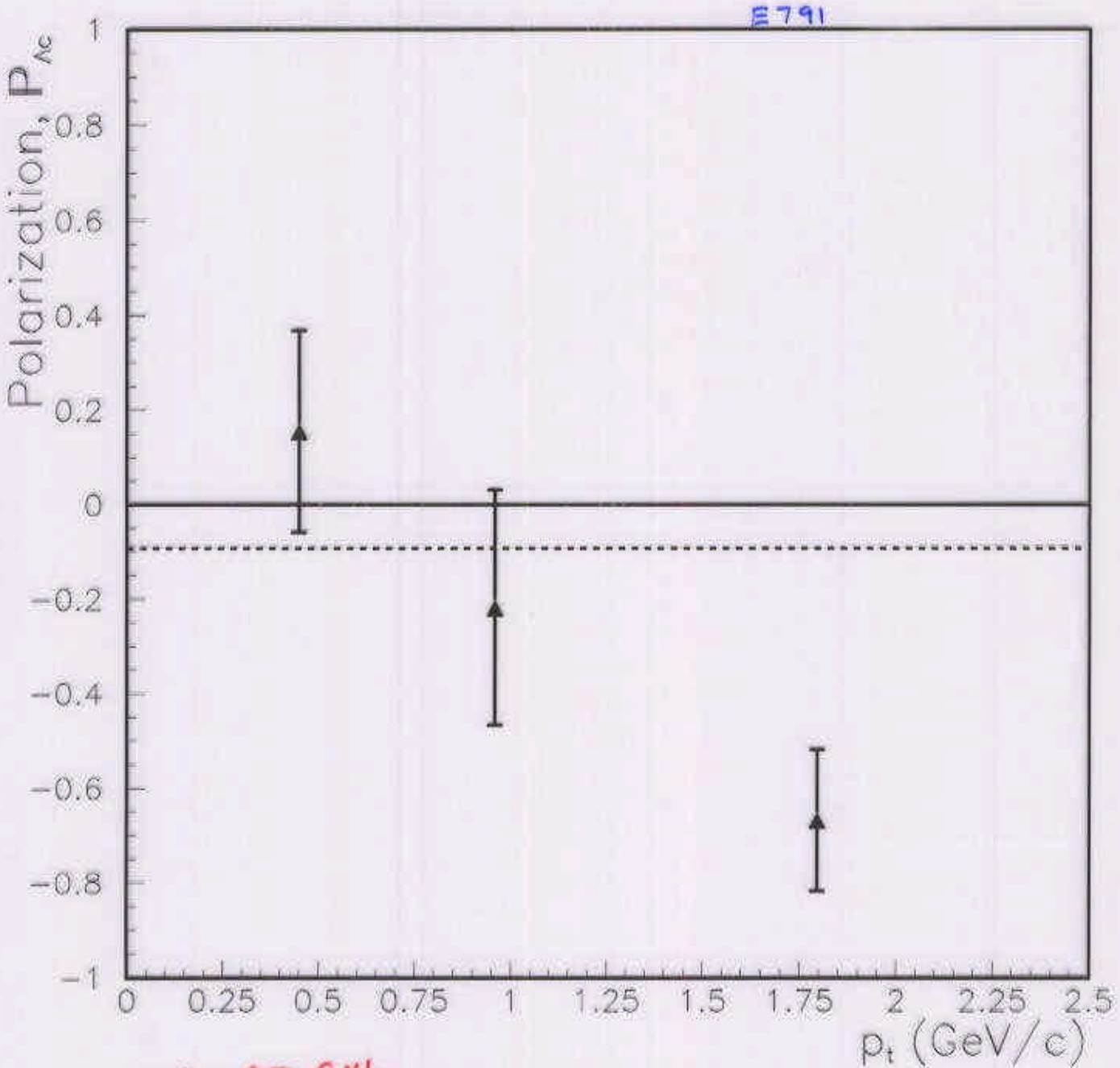

$0 < p_T < 0.71$ GeV/c

$0.71 < p_T < 1.24$ GeV/c

$1.24 < p_T < 5.20$ GeV/c

E791

SYSTEMATIC ERRORS

Mode	Fit 3p	Čerenkov(%)	Production(%)	DC hole(%)	2d Tweak(%)
$\bar{K}^{*0}$	19.5±2.6	18.9±2.7	19.5±2.7	21.2±3.0	19.8±2.8
Δ^{++}	18.0±2.9	16.8±2.8	18.1±2.9	20.5±3.3	17.3±2.9
$\Lambda(1520)$	7.7±1.8	8.3±1.9	7.6±1.8	6.8±1.7	7.3±1.8
Nonresonant	54.8±5.5	55.9±5.8	54.9±5.7	51.6±6.5	55.7±5.8

Table 10.2: The fit fractions for the decay $\Lambda_c \to pK\pi$ from the MINUIT fit.

Mode	Ckv(%)	Prod(%)	DC hole(%)	2d Tweak(%)	Syst Error (%)
$p\bar{K}^{*0}$	-0.6	0.0	+1.7	+0.3	1.8
$\Delta^{++}K^-$	-1.2	+0.1	+2.5	-0.7	2.9
$\Lambda(1520)\pi^+$	+0.5	-0.1	+0.9	-0.4	1.1
Nonres	+1.1	+0.1	-3.2	+0.9	3.5

Table 10.3: Deviations from the fit 3p fit fractions for the Systematic Errors.

The $\pi^+\pi^-\pi^+$ Invariant mass

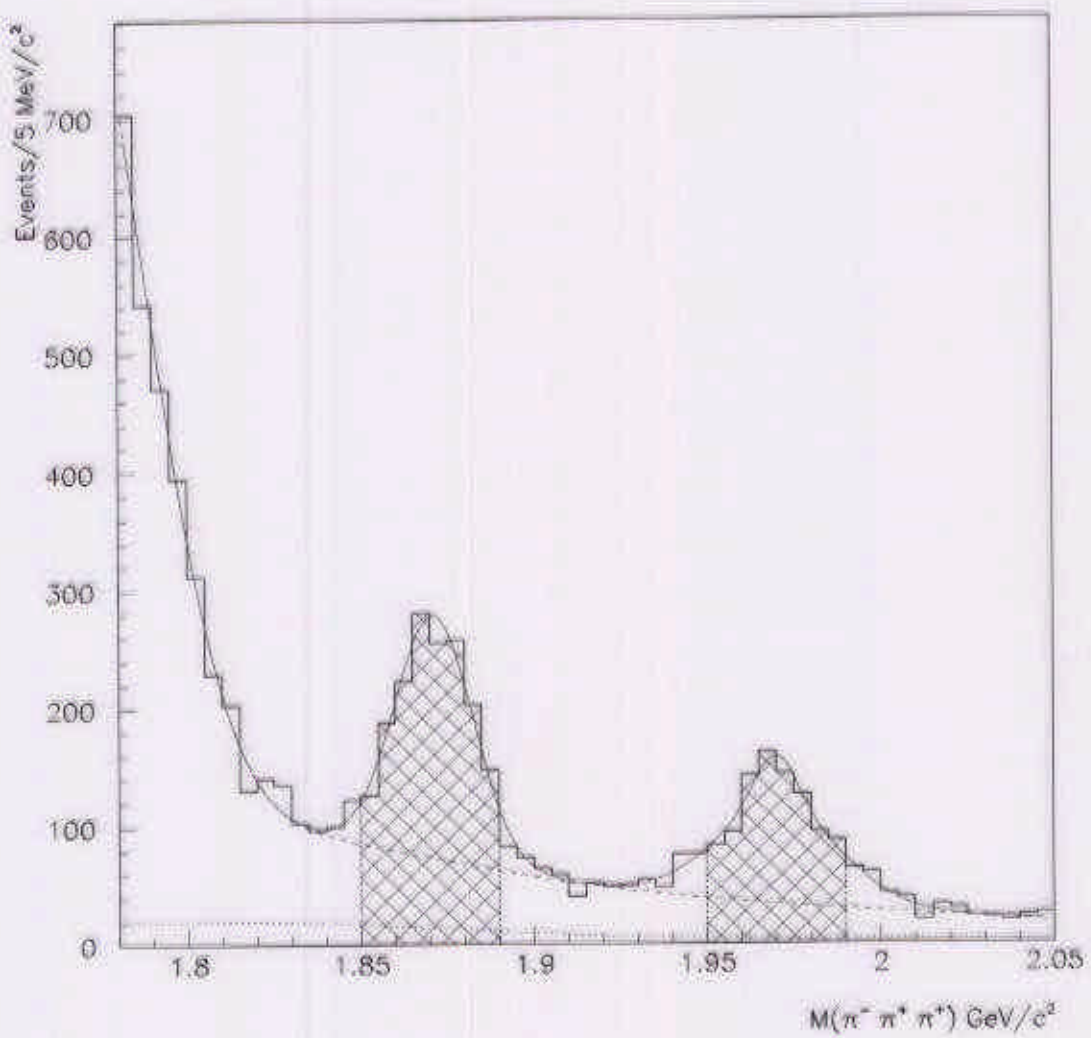

Figure 1: The $\pi^+\pi^-\pi^+$ spectrum with the final set of cuts.

To perform the Dalitz plot analysis we have:

1172 ± 61 events in the D^+ mass region

848 ± 44 events in the D_s^+ mass region

$D_s^+ \to \pi^+\pi^-\pi^+$ Dalitz plot analysis

Dipions resonances

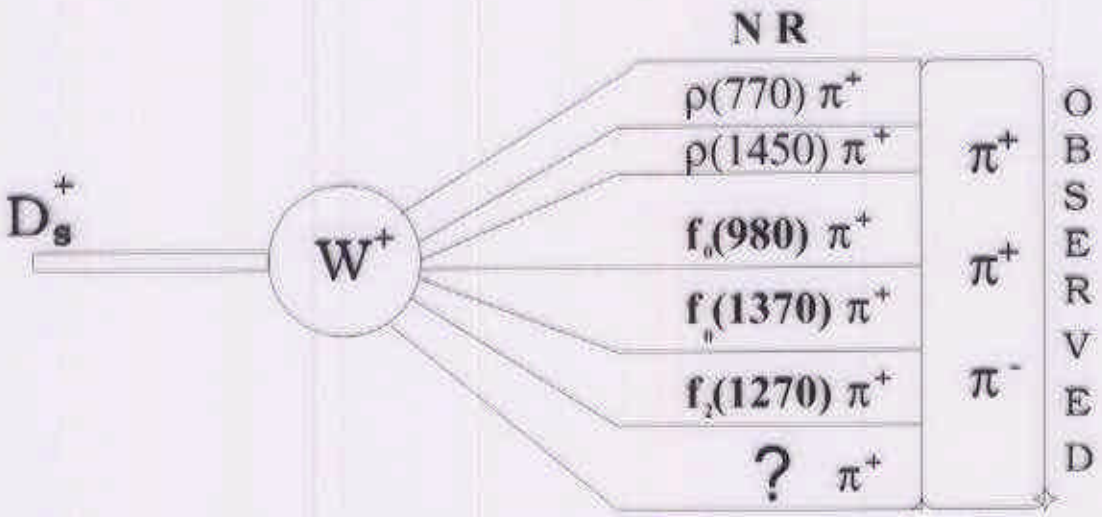

Figure 2: Possible final states for D_s^+ decays to $\pi^+\pi^-\pi^+$

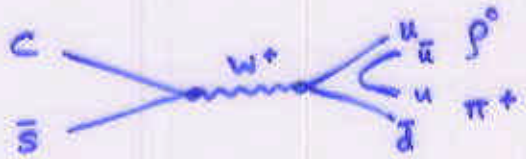

$D_s^+ \to \pi^+\pi^-\pi^+$

$M^2_{\pi^+\pi^-}$ and $M^2_{\pi_1^+\pi^-}$ vs $M^2_{\pi_2^+\pi^-}$ data distributions

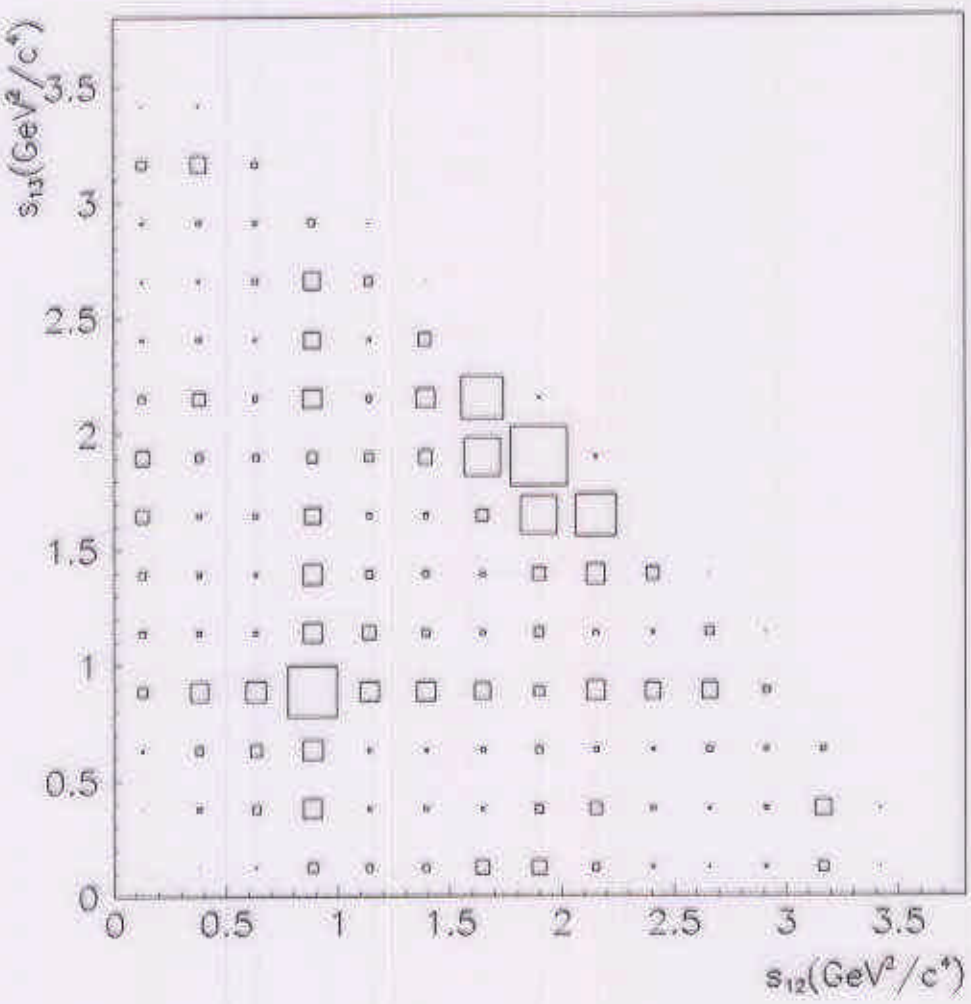

Figure 3: 1- and 2-D dipion mass distributions

Amplitude.

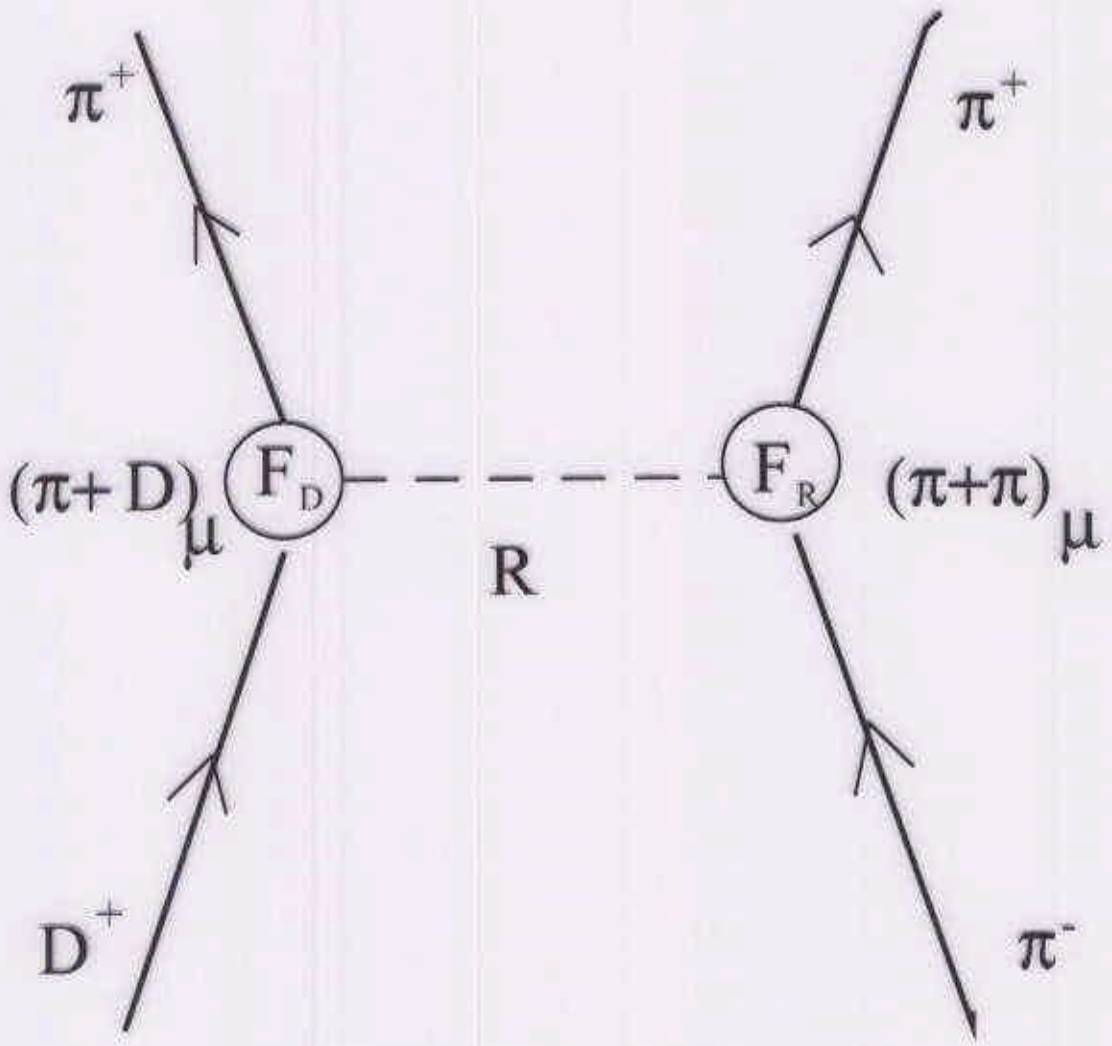

Figure 4: The $D^+ \to \pi^+\pi^-\pi^+$ decay.

$$\mathcal{M} = \sum_j \mathbf{c_j}\, \mathbf{e}^{\mathbf{i}\delta_\mathbf{j}}\; F_d\; \mathcal{BW}_j\; F_{Rj}\; \mathcal{P}(cos\Theta)_j \;+\; \mathbf{c_{NR}}\; \mathbf{e}^{\mathbf{i}\delta_{\mathbf{NR}}}$$

- $\mathbf{c_j\ e^{i\delta_j}}$ and $\mathbf{c_{NR}\ e^{i\delta_{NR}}} \rightarrow$ fit parameters

- $\mathcal{BW}_j = \dfrac{\mathbf{1}}{\mathbf{m_{ik}^2 - m_0^2 + i m_0 \Gamma(m)}}$

$$\Gamma(m) = \Gamma_0 \frac{m_0}{m} \left(\frac{p^*}{p_0^*}\right)^{2J+1} \frac{F_R^2(p^*)}{F_R^2(p_0^*)}$$

- $\mathcal{P}(cos\Theta)_j \rightarrow$ Angular Distribution
- F_D and $F_R \rightarrow$ Blatt-Weisskopf form factors

Fit with mass and width free

Non well determined mass and width parameters PDG(98):

- $f_0(1370)$:
  M = 1200 to 1500MeV Γ_0= 200 to 500 MeV
- $f_0(980)$:
  M = 980 $\pm$ 10 MeV Γ_0 = 40 to 100 MeV

We used the Flatté parametrization for the $f_0(980)$ resonance, due the possibility of the $f_0(980) \to KK$,

$$\mathcal{BW} = \frac{1}{\mathbf{m}^2_{\pi\pi} - \mathbf{m}_0^2 + \mathbf{i}\mathbf{m}_0(\mathbf{\Gamma}_\pi(\mathbf{m}) + \mathbf{\Gamma}_\mathbf{K}(\mathbf{m}))}$$

$$\Gamma_\pi(m) = \mathbf{g}_\pi \sqrt{m^2_{\pi\pi}/4 - m^2_\pi}$$

and

$$\Gamma_K(m) = \mathbf{g}_\mathbf{K}/2 \; (\sqrt{m^2_{\pi\pi}/4 - m^2_{K^+}} + \sqrt{m^2_{\pi\pi}/4 - m^2_{K^0}})$$

Results for $D_s^+ \to \pi^+\pi^-\pi^+$

Minimizing **FCN** $= -2ln(\mathcal{L})$:

- $f_0(1370)$: M $= 1434 \pm 18 \pm 9$ MeV, $\Gamma = 172 \pm 32 \pm 6$ MeV
- $f_0(980)$ M $= 977 \pm 3 \pm 2$ MeV
- $g_K = 0.02 \pm 0.04 \pm 0.03$ and $g_\pi = 0.09 \pm 0.01 \pm 0.01$
- **WA76** $g_K = 0.56 \pm 0.18$ and $g_\pi = 0.28 \pm 0.04$
- Regular Breit Wigner $\to \Gamma_0 = 44 \pm 5 \pm 2$ MeV

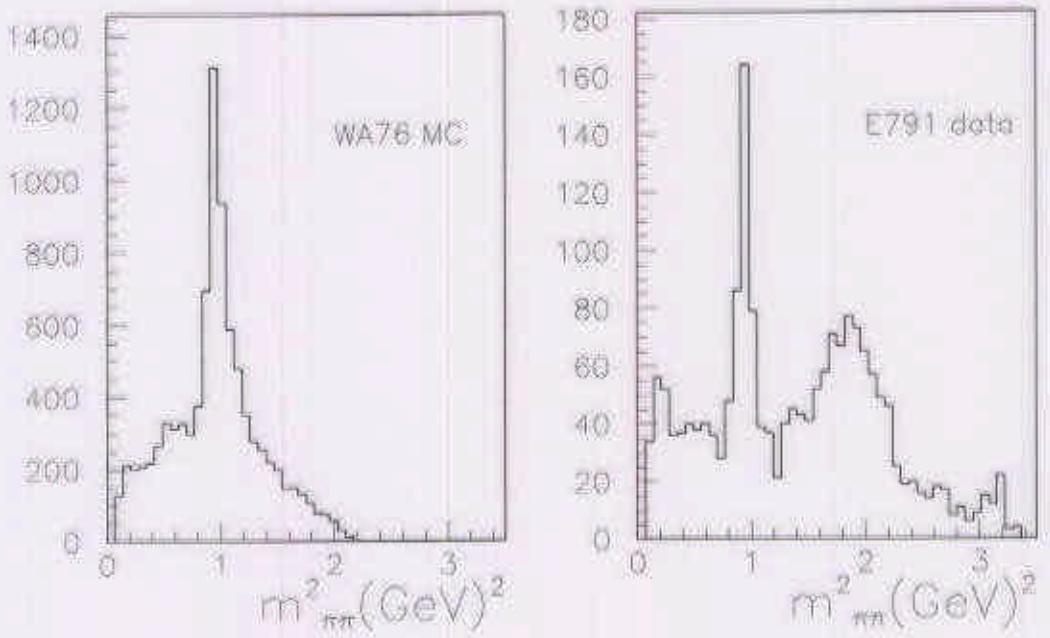

Figure 5: Pi-Pi mass-squared

Phases and fractions

The fraction is defined by:

$$f_i = \frac{\int dm_{12}^2 dm_{23}^2 \mid c_i e^{i\delta_i} \mathcal{M}_i \mid^2}{\int dm_{12}^2 dm_{23}^2 \mid \Sigma c_j e^{i\delta_j} \mathcal{M}_j \mid^2}$$

- Dominant isoscalar resonances $f_0(980)$ and $f_0(1370)$,

mode	phase (degree)	fraction(%)
$f_0(980)\pi^+$	0°(fixed)	$56.5 \pm 4.3 \pm 4.7$
non-resonant	$(181 \pm 94 \pm 51)°$	$0.5 \pm 1.4 \pm 1.7$
$\rho^0(770)\pi^+$	$(109 \pm 24 \pm 5)°$	$5.8 \pm 2.3 \pm 3.7$
$f_2(1270)\pi^+$	$(133 \pm 13 \pm 28)°$	$19.7 \pm 3.3 \pm 0.6$
$f_0(1370)\pi^+$	$(198 \pm 19 \pm 27)°$	$32.4 \pm 7.7 \pm 1.9$
$\rho^0(1450)\pi^+$	$(162 \pm 26 \pm 17)°$	$4.4 \pm 2.1 \pm 0.2$

almost 90%.

- Negligible Non-Resonant contribution.

- Possible $\rho^0(770)$.

Goodness of the fit

With these parameters, we generated a mini-MC and compared with data.

$$\chi^2/DOF = 71.8/68 \rightarrow CL = 35\%$$

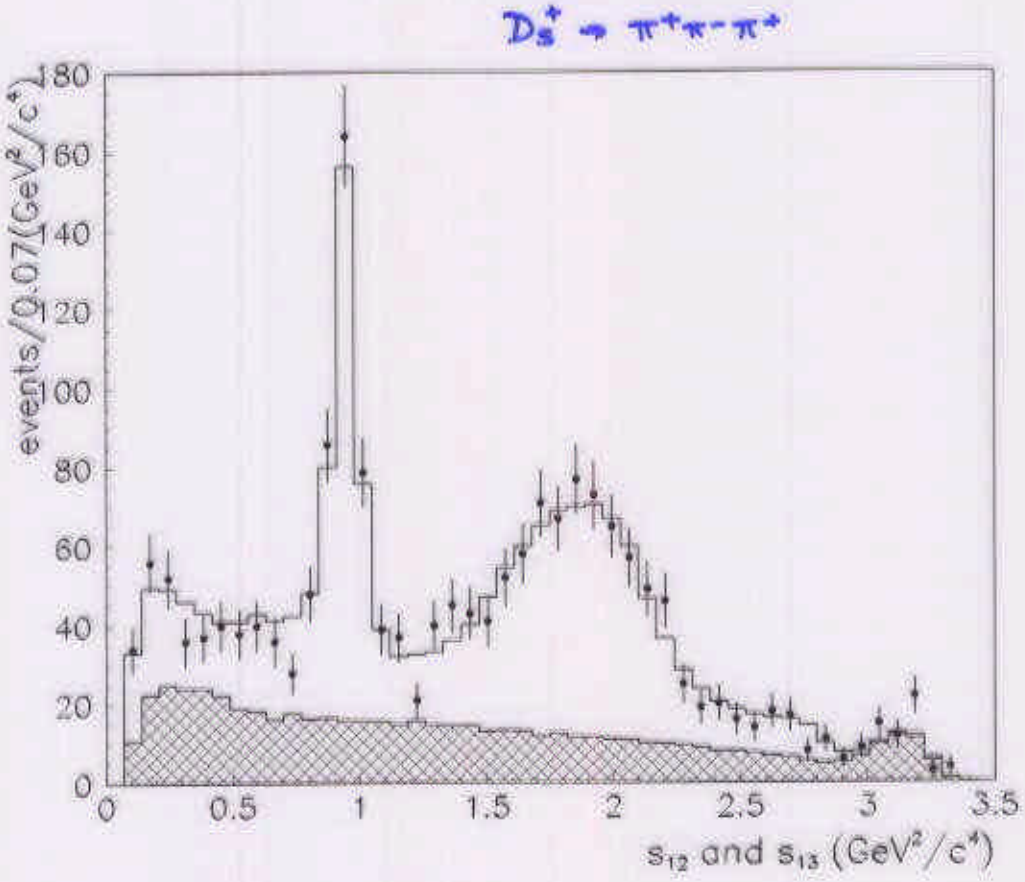

Figure 6: Pi-Pi mass-squared: data and fit.

$D^+ \to \pi^+\pi^-\pi^+$ Dalitz plot analysis

Data distributions

What is the origin of the low mass peak?

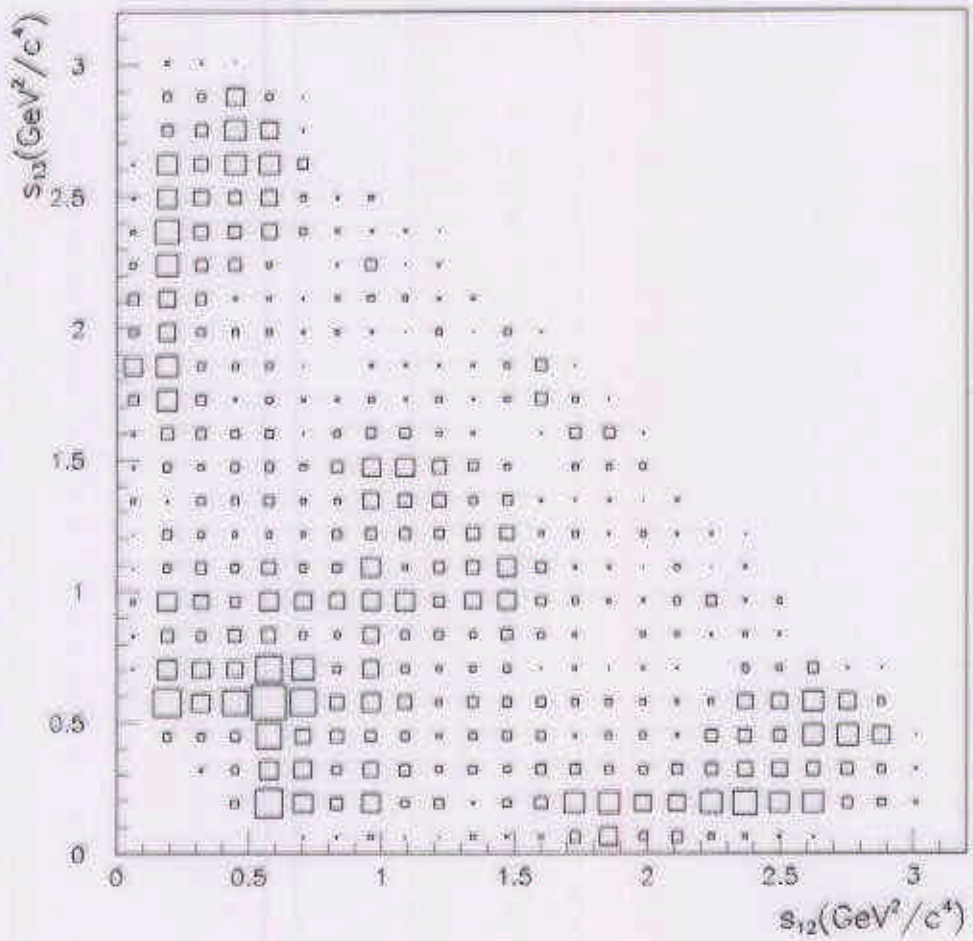

Figure 7: Pi-Pi mass-squared: 1- and 2-D distributions, D^1.

- Peculiar distribution of the known dipion resonances with their possibles interferences?
- New dipion resonance with mass below the $\rho(770)$?

Results for $D^+ \to \pi^+\pi^-\pi^+$

First approach

Initial fit with the same states used in the D_s^+.

mode	phase (degree)	fraction(%)
$\rho^0(770)\pi^+$	0°(fixed)	20.8 ±2.4
non-resonant	$(150.1 \pm 11.5)°$	38.6 ±9.7
$f_0(980)\pi^+$	$(151.8 \pm 16)°$	7.4 ± 1.4
$f_2(1270)\pi^+$	$(102.6 \pm 16.0)°$	6.3 ±1.9
$f_0(1370)\pi^+$	$(143.2 \pm 9.7)°$	10.7 ±3.1
$\rho^0(1450)\pi^+$	$(45.8 \pm 14.9)°$	22.6 ±3.7

- Dominant Non-resonant contribution.
- The $\rho^0(1450)\pi^+$ and $\rho^0(770)\pi^+$ contributions are comparable.
- Compatible with E687 results.

Goodness of the fit

$$\chi^2/DOF = 254/162 \;\rightarrow\; CL = 10^{-5}$$

- This model, with the known resonances, **is not enough** to explain our experimental data.
- We need a new dipion resonance with mass below the $\rho^0(770)$.
- The only available state is the long suspected particle σ.

Results for $D^+ \to \pi^+\pi^-\pi^+$

Second approach, including the σ

- $\Delta FCN = -2(\ln \mathcal{L}_\sigma - \ln \mathcal{L}_0) = 118$
- **Mass** $478^{+24}_{-23} \pm 17$ **MeV**
- **Width** $324^{+42}_{-40} \pm 21$**MeV**

$D^+ \to \pi^+\pi^-\pi^+$ fit with a σ

mode	phase (degree)	fraction(%)
$\sigma\pi^+$	$(205.7 \pm 8.0 \pm 5.2)^\circ$	$46.3 \pm 9.0 \pm 2.1$
$\rho^0(770)\pi^+$	0°(fixed)	$33.6 \pm 3.2 \pm 2.2$
non-resonant	$(57.3 \pm 19.5 \pm 5.7)^\circ$	$7.8 \pm 6.0 \pm 2.7$
$f_0(980)\pi^+$	$(165.0 \pm 10.9 \pm 3.4)^\circ$	$6.2 \pm 1.3 \pm 0.4$
$f_2(1270)\pi^+$	$(57.3 \pm 7.5 \pm 2.9)^\circ$	$19.4 \pm 2.5 \pm 0.4$
$f_0(1370)\pi^+$	$(105.4 \pm 17.8 \pm 0.6)^\circ$	$2.3 \pm 1.5 \pm 0.8$
$\rho^0(1450)\pi^+$	$(319.1 \pm 39.0 \pm 10.9)^\circ$	$0.7 \pm 0.7 \pm 0.3$

- Dominant isoscalar resonance $\sigma(500)$.
- Low Non-Resonant contribution.
- The $\rho^0(770)$ contribution remains strong but the $\rho^0(1450)$ becomes negligible.

Goodness of the fit

$$\chi^2/DOF = 138/162 \rightarrow CL = 85\%$$

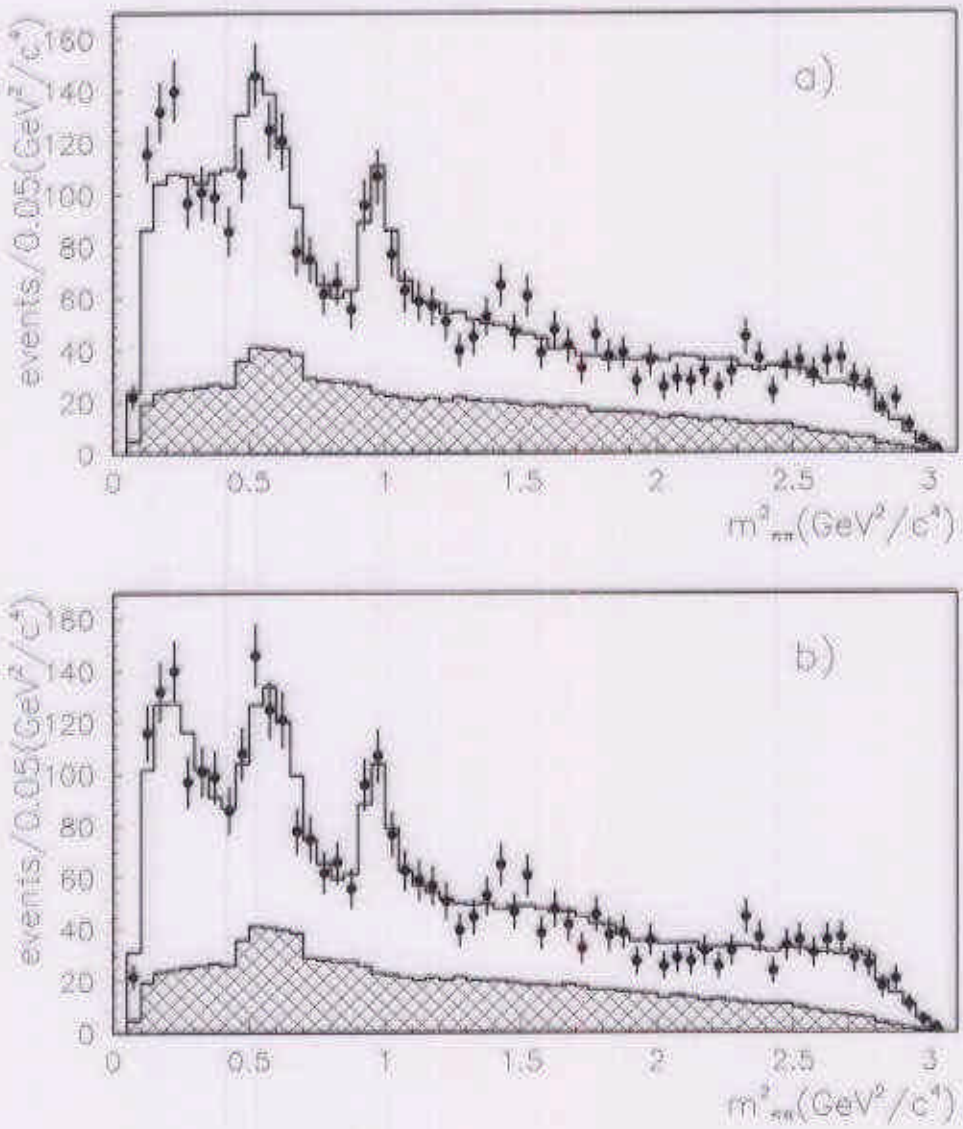

Figure 9: Pi-Pi mass-squared: data and sigma fit, D^+.

Additional tests

1 Toy model

Breit Wigner with no phase

$$BW_T = \sqrt{\frac{1}{(m^2 - m_0^2 + im_0\Gamma(m))^2}}$$

- Well defined mass 434 $\pm$11 MeV/c^2 and width 267 $\pm$ 37 MeV/c^2.
- The relative phase of the $\sigma\pi^+$ relatively to the $\rho^0(770)\pi^+$ shifted about $\pi/2$.
- Strong interference generates a large non resonant amplitude, leading to unphysically large sum fractions.
- $\Delta FCN = -2(\ln \mathcal{L}_\sigma - \ln \mathcal{L}_{Toy}) = 15$.

2 σ as vector particle

- Poorly defined mass 805 ± 194 MeV and width 1438 ± 903 MeV
- $\Delta FCN = 66$

3 σ as tensor particle

- Poorly defined mass 2350 ± 683 MeV$/c^2$ and non physics width -690 ± 1033.
- $\Delta FCN = 13$

Conclusions

We observe significant polarization of the Λ_c^+ as a function of p_T^2.

We observe an insignificant asymmetry in the $f_0(980)$ Breit Wigner.

We find strong evidence for a light and broad scalar resonance in $D^+ \to \pi^+\pi^-\pi^+$ decay.